

Molecular mechanisms of cobalt-catalyzed hydrogen evolution

Smaranda C. Marinescu, Jay R. Winkler¹, and Harry B. Gray¹

Division of Chemistry and Chemical Engineering, Beckman Institute, California Institute of Technology, Pasadena, CA 91125

Contributed by Harry B. Gray, August 6, 2012 (sent for review July 19, 2012)

Several cobalt complexes catalyze the evolution of hydrogen from acidic solutions, both homogeneously and at electrodes. The detailed molecular mechanisms of these transformations remain unresolved, largely owing to the fact that key reactive intermediates have eluded detection. One method of stabilizing reactive intermediates involves minimizing the overall reaction free-energy change. Here, we report a new cobalt(I) complex that reacts with tosylic acid to evolve hydrogen with a driving force of just 30 meV/Co. Protonation of Co^I produces a transient Co^{III}-H complex that was characterized by nuclear magnetic resonance spectroscopy. The Co^{III}-H intermediate decays by second-order kinetics with an inverse dependence on acid concentration. Analysis of the kinetics suggests that Co^{III}-H produces hydrogen by two competing pathways: a slower homolytic route involving two Co^{III}-H species and a dominant heterolytic channel in which a highly reactive Co^{II}-H transient is generated by Co^I reduction of Co^{III}-H.

catalysis | renewable fuel

Hydrogen (H₂) is a clean and renewable fuel (1–4). Hydrogenase enzymes that contain iron and nickel cofactors evolve hydrogen catalytically from water near the thermodynamic potential with turnover frequencies as high as 9,000 s⁻¹ at 30 °C (5, 6). However, the large size and relative instability of these enzymes under aerobic conditions has led to the search for well-defined molecular catalysts that can produce hydrogen from water in a nonbiological system. Platinum is an excellent catalyst for proton reduction and hydrogen oxidation, but its scarcity and high cost limit widespread use. These considerations have led to the development of molecular catalysts that employ earth-abundant metals (7–11).

Synthetic complexes of nickel (12–15), cobalt (16–26), iron (27–29), and molybdenum (30–32) have been developed recently as electrocatalysts for the production of hydrogen. Co-diglyoxime complexes have been shown to generate hydrogen from protic solutions at relatively modest overpotentials. Given the broad interest and potential application in artificial photosynthesis, the mechanism of hydrogen formation has been the subject of many experimental (16, 18, 33–40) and theoretical (41–43) investigations. Several pathways have been proposed (Fig. 1), all beginning with protonation of a Co^I complex to form Co^{III}H. H₂ evolution can occur via protonation of Co^{III}H or upon bimolecular combination of two Co^{III}H species. Alternatively, Co^{III}H can be reduced by Co^I to a mixture of Co^{II}H and Co^{II}. The generated Co^{II}H can react via similar heterolytic or homolytic pathways to generate H₂. The key intermediate in these transformations (Co^{III}H) has, until now, not been observed directly. We report here the results of extensive kinetics studies that shed new light on the mechanism of proton reduction.

The triphos ligand (1,1,1-tris(diphenylphosphinomethyl)ethane) allows for facile tuning of reduction potentials by introduction of electron-withdrawing or electron-donating aryl groups into the framework. Several Co(triphos) species have been synthesized (44–47): protonation of [(PP₃)CoH] (48) (PP₃ = P(CH₂CH₂PPh₂)₃) led to the formation of the dihydride complex, [(PP₃)Co(H)₂][PF₆] (49–51); and two [(triphos)Co^{III}(H)₂]⁺ species also have been fully characterized (52, 53).

Results and Discussion

Synthesis and Cyclic Voltammetry. Upon treatment with triphos, cobalt(II) iodide undergoes spontaneous reduction to Co(triphos) (I) (**1**), a pink solid (*SI Appendix*, Fig. S1) (54). Crystal structure analysis of **1** reveals pseudotetrahedral geometry at Co^I (*SI Appendix*, Fig. S2). The iodide can be abstracted with TlPF₆ in 5:1 tetrahydrofuran:acetonitrile (THF:CH₃CN), to generate the cationic adduct [Co(triphos)(CH₃CN)][PF₆] (**2**) as a blue solid. The solid-state structure of **2** exhibits pseudotetrahedral geometry at the metal (Fig. 1), with the PF₆⁻ counter ion outside the coordination sphere.

Cyclic voltammograms of **2** at a glassy carbon electrode in a 0.1 M CH₃CN solution of [nBu₄N][PF₆] feature a reversible wave at E_{1/2} = -0.68 V versus Fc⁺⁰ (*) assigned to the Co^{II/I} couple, and an irreversible oxidation at +0.66 V assigned to Co^{III/II} (Fig. 2 and *SI Appendix*). An irreversible reduction wave at -1.81 V is assigned to Co^{I/0}, and the irreversible wave at -2.73 V is assigned to Co^{0/-1} (cyclic voltammograms of **1** are included in the *SI Appendix*). Voltammograms of **2** with varying amounts of *p*-toluenesulfonic acid monohydrate [TsOH•H₂O, pK_a = 8.7 in acetonitrile (55)] exhibit enhanced currents at potentials near that for the Co^{II/I} couple; the currents increased markedly at more negative potentials (reduction of Co^I) and at higher acid concentrations (Fig. 2). Cyclic voltammetry experiments performed in the absence of catalyst **2**, or in the absence of the metal center (*SI Appendix*), produced no catalytic current, suggesting that **2** catalyzes H₂ evolution. A maximum value of 9.5 for the ratio of the catalytic current to the peak current in the absence of acid (*i*_{cat}/*i*_p, E = -1.8 V) was determined at an acid concentration of 14.7 mM, corresponding to an apparent turnover frequency of 1.8(2) × 10¹ s⁻¹ at 25 °C (12, 56). Bulk electrolysis of a 0.3 mM solution of **2** in the presence of 6.0 mM TsOH•H₂O in 65 mL 0.1 M acetonitrile solution of [nBu₄N][PF₆] at -1.0 V consumed 9.2 coulombs of charge after 2 h. Analysis of the gas mixture in the headspace of the electrolysis cell by gas chromatography confirmed production of H₂ with a faradaic yield of 99 ± 10%.

Characterization of Co^{III}-H. Addition of five equivalents of TsOH•H₂O in CD₃CN to a solution of **2** led to an immediate color change from blue to yellow/green. A singlet at δ 4.58 ppm was observed in the ¹H NMR spectrum of the reaction mixture, suggesting formation of H₂. The experiment was repeated in a

Author contributions: S.C.M. designed research; S.C.M. performed research; S.C.M. contributed new reagents/analytic tools; S.C.M., J.R.W., and H.B.G. analyzed data; and S.C.M., J.R.W., and H.B.G. wrote the paper.

The authors declare no conflict of interest.

Data deposition: The atomic coordinates have been deposited in the Cambridge Structural Database, Cambridge Crystallographic Data Centre, Cambridge CB2 1EZ, United Kingdom <http://www.ccdc.cam.ac.uk>, [CSD reference numbers 838815 (1), 844589 (2), and 846384 (3)].

*All electrode potentials are reported relative to the ferricenium/ferrocene (Fc⁺⁰) couple.

¹To whom correspondence may be addressed. E-mail: winklerj@caltech.edu or hbgray@caltech.edu.

This article contains supporting information online at www.pnas.org/lookup/suppl/doi:10.1073/pnas.1213442109/-DCSupplemental.

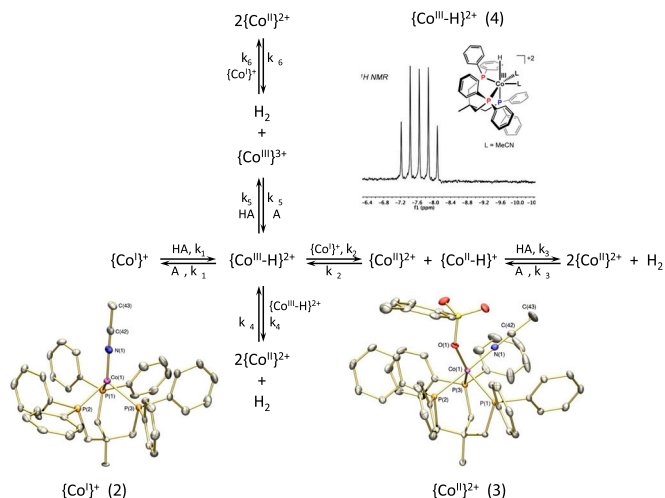


Fig. 1. Reaction pathways for the evolution of H_2 from the reaction of a Co^{I} complex with acid (HA). Models based on the X-ray crystal structures of Co^{I} (**2**) and Co^{II} (**3**) triphos complexes appear in the lower portion of the figure. Thermal ellipsoids are drawn at 50% probability; hydrogen atoms, out-of-sphere anions, and solvent molecules are omitted for clarity. The ^1H NMR spectrum and structural model of the $\text{Co}^{\text{III}}\text{-H}$ (**4**) intermediate formed in the reaction of **2** with $\text{TsOH}\cdot\text{H}_2\text{O}$ appear in the upper right.

70 mL round bottom flask and allowed to stir at room temperature for 5 h. Analysis of the gas mixture in the headspace of the flask by gas chromatography confirmed production of 0.5 equivalents of H_2 . Broad, paramagnetically shifted peaks were detected in the ^1H NMR spectrum of the reaction mixture, suggesting the formation of Co^{II} . Recrystallization of the reaction mixture by vapor diffusion with diethyl ether led to the formation of yellow/green crystals. An X-ray structural study confirmed formation of a Co^{II} complex containing a coordinated tosylate anion (**3**), with another tosylate outside the coordination sphere (Fig. 1). We conclude that protonation of the cationic Co^{I} species leads to H_2 evolution with consequent oxidation to Co^{II} . Cyclic voltammetry results for **3** are included in the *SI Appendix*. The reverse reaction, the oxidation of H_2 by Co^{II} , was investigated as well. Addition of H_2 (1 atm) to a 16.4 mM acetonitrile solution of **3** led slowly to formation of broad, paramagnetically shifted peaks at δ 15.40, -0.77 , and -1.45 ppm (26% conversion after 1 d), consistent with formation of **2**.

^1H NMR spectra recorded immediately after mixing a solution of **2** with 10 equivalents of $\text{TsOH}\cdot\text{H}_2\text{O}$ revealed a doublet of triplets at δ -7.64 ppm (Fig. 1), and the coupling constants ($J_{\text{cis-P-H}} = 65$ Hz; $J_{\text{trans-P-H}} = 130$ Hz) accord with a Co-H complex (57–60), $\{(\text{triphos})\text{CoH}(\text{CH}_3\text{CN})_2\}^{2+}$ (**4**). The $^{31}\text{P}\{^1\text{H}\}$ NMR spectrum displays two peaks at δ 37.3 and -1.7 ppm in a

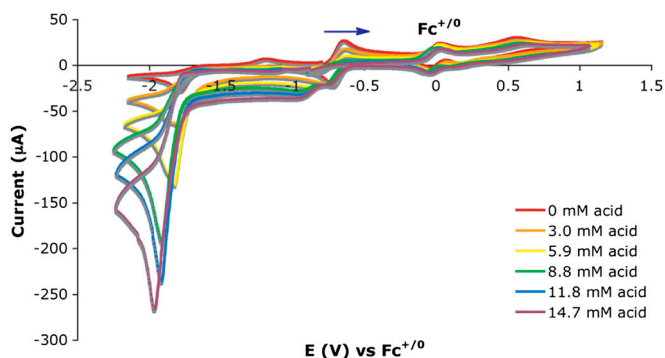


Fig. 2. Cyclic voltammograms of **2** (1.3 mM) in acetonitrile solution containing 0.1 M $[\text{nBu}_4\text{N}][\text{PF}_6]$ in the presence of $\text{TsOH}\cdot\text{H}_2\text{O}$ and ferrocene. Scan rate: 100 mV s^{-1} ; glassy carbon electrode.

2:1 ratio, confirming the assignment (*SI Appendix*, Fig. S17C). The equilibrium constant for the protonation reaction (Fig. 1: $K_1 = k_1/k_{-1}$) was determined from measurements of the variation of the $\text{Co}^{\text{III}}\text{-H}$ concentration with $[\text{TsOH}\cdot\text{H}_2\text{O}]$ by integration of the Co-H ^1H NMR signal relative to a dihydroanthracene internal standard (Table 1). At higher acid concentrations, nearly constant apparent K_1 values (approximately 0.2) are observed (Table 1, entries 2–5), corresponding to a $\text{p}K_a$ value of 8.0(8) for $\text{Co}^{\text{III}}\text{-H}$ in CH_3CN .

Kinetics. ^1H NMR spectra provided a convenient probe of the kinetics of conversion of $\text{Co}^{\text{III}}\text{-H}$ to **3**. The $\text{Co}^{\text{III}}\text{-H}$ concentration exhibits an inverse dependence on reaction time (25 °C; $[\text{2}]_0 = 16.4$ mM; $[\text{TsOH}\cdot\text{H}_2\text{O}]_0 = 0.164$ M; dihydroanthracene internal standard), consistent with a reaction that is second order in the concentration of $\text{Co}^{\text{III}}\text{-H}$ (Fig. 3), and a factor of two decrease in reaction half-life upon doubling $[\text{2}]_0$ supports this interpretation. Greater acid concentrations lead to slower reactions (Table 1), yet, over the 0.082–0.656 M $\text{TsOH}\cdot\text{H}_2\text{O}$ concentration range, the kinetics remain second order in $[\text{Co}^{\text{III}}\text{-H}]$. Second-order rate constants were determined at four different temperatures (15, 25, 35, and 45 °C; $[\text{2}]_0 = 16.4$ mM; $[\text{TsOH}\cdot\text{H}_2\text{O}]_0 = 0.164$ M; *SI Appendix*, Table S1) and activation parameters were extracted from an Eyring plot ($\Delta H^\ddagger = 25.0 \pm 0.9$ kcal mol^{-1} ; $\Delta S^\ddagger = 17.9 \pm 2.8$ eu; *SI Appendix*, Fig. S19). The $^{31}\text{P}\{^1\text{H}\}$ nuclear magnetic resonance (NMR) measurements (using Ph_4PBr in a sealed capillary as an internal standard) of the $\text{Co}^{\text{III}}\text{-D}$ (prepared from **2** and $\text{TsOD}\cdot\text{D}_2\text{O}$) decay kinetics revealed that the isotope effect, $k_{\text{obsH}}/k_{\text{obsD}}$, varied with acid concentration up to a maximum value of 0.57 (Table 1).

Cyclic voltammetric measurements indicate that both Co^{I} and Co^0 complexes will effect proton reduction. The thermodynamic potential for hydrogen evolution using $\text{TsOH}\cdot\text{H}_2\text{O}$ is -0.65 V (55), corresponding to a 30-meV/Co driving force for proton reduction by Co^{I} . These energetics are consistent with experiments in which H_2 is evolved from acidic solutions of **2**, and **2** is regenerated from **3** in the presence of excess H_2 .

Our observation of $\text{Co}^{\text{III}}\text{-H}$ has opened the way for direct probing of the mechanisms proposed for Co-catalyzed H_2 evolution (Fig. 1). The second-order kinetics suggest that H_2 elimination in a bimolecular reaction between two $\text{Co}^{\text{III}}\text{-H}$ complexes could be a dominant pathway (k_4 , Fig. 1). But, since the specific rate of this reaction should be independent of acid concentration, the observed inverse acid dependence demonstrates that there is a competing pathway. Direct protonation of $\text{Co}^{\text{III}}\text{-H}$ to produce Co^{III} and H_2 is inconsistent with both the second-order kinetics and the decreasing rate constant with increasing acid concentration.

The third pathway for H_2 evolution from Co^{I} in acid involves reduction of $\text{Co}^{\text{III}}\text{-H}$ to a $\text{Co}^{\text{II}}\text{-H}$ complex. In our kinetics experiments, the only available reductant is Co^{I} (**2**), so the position of the protonation equilibrium in the $\text{Co}^{\text{II}}\text{-H}$ pathway will have a substantial impact on the observed kinetics (the inverse acid dependence can be explained by the absence of Co^{I} at higher acid concentrations). In the limit of rapid equilibrium between Co^{I} and $\text{Co}^{\text{III}}\text{-H}$, and irreversible following reactions, we predict that the disappearance of $\text{Co}^{\text{III}}\text{-H}$ will obey second-order kinetics with an observed rate constant given by Eq. 1. Using the data in Table 1, we can estimate that $k_4 = 2.5 \times 10^{-3}$ $\text{M}^{-1} \text{s}^{-1}$ and $k_2 = 4.4 \times 10^{-2}$ $\text{M}^{-1} \text{s}^{-1}$. Numerical simulations of the reaction kinetics defined by the model outlined in Fig. 1 indicate that 2.5×10^{-3} $\text{M}^{-1} \text{s}^{-1}$ is an upper limit for k_4 and $k_2 \sim 5 \pm 1 \times 10^{-2}$ $\text{M}^{-1} \text{s}^{-1}$ (*SI Appendix*) and that over the acid concentration that we examined, H_2 evolution proceeds almost exclusively via the pathway involving $\text{Co}^{\text{II}}\text{-H}$. This conclusion is bolstered by cyclic voltammetry, wherein large catalytic currents do not occur until potentials consistent with Co^0 (or $\text{Co}^{\text{II}}\text{-H}$ in the presence of acid) formation are achieved. The large and positive entropy

Table 1. Results of kinetics studies of the reaction of 2 with TsOH•H₂O

Entry	[TsOH•H ₂ O] (M)*	[Co ^{III} -H] ₀ (mM) [†]	K ₁	k _{obsH} (M ⁻¹ s ⁻¹) [†]	KIE (k _{obsH} /k _{obsD})
1	0.082	7.1 [‡]	0.07(9)	0.064(6)	0.19(4)
2	0.164	11.5	0.18(3)	0.024(2)	0.41(4)
3	0.328	13.6	0.21(2)	0.014(1)	0.56(4)
4	0.492	14.3	0.20(2)	0.012(1)	-
5	0.656	14.8	0.21(2)	0.010(1)	0.57(4)

* [Co^I]₀ = 16.4 mM; 0.7 mL CD₃CN; 25 °C.[†] Average of two runs.[‡] The lower value for K₁ observed at 82 mM acid concentration is likely due to partial reaction of Co^{III}-H prior to the nuclear magnetic resonance measurement, as the measured rate constant for the entry 1 is higher than the one for entries 2–5.

of activation is likely due to the solvent dissociation from [(triphos)CoH(CH₃CN)₂]²⁺ (**4**). The values observed for the

$$k_{\text{obs}} = 2k_4 + \frac{k_{-1}k_2[\text{A}^-]}{k_1[\text{HA}]}, \quad [1]$$

kinetic isotope effect are difficult to assess due to a combination of protonation and electron transfer processes.

Armed with rate and equilibrium constants for the homogeneous evolution of H₂ from Co^I, we undertook numerical simulations of the cyclic voltammetry data. These simulations can be particularly challenging, owing to the large number of parameters involved in modeling the kinetics and the limited number of available observables. Nevertheless, we have found a set of parameters that describes the cyclic voltammetry of **2** in the presence of TsOH•H₂O that is also consistent with the simulations of the homogeneous kinetics (SI Appendix, Figs. S4, S7, and S8). Of particular interest is the large specific rate (10⁷ M⁻¹ s⁻¹) estimated for the reaction of Co^{II}-H with TsOH•H₂O. The comparable value for the reaction of a Co^{II}(H)-diglyoxime complex with 6-bromo-2-naphthol (pK_a ~ 26.1) is 4 × 10⁴ M⁻¹ s⁻¹ (36).

Our homogeneous and electrochemical kinetics analyses demonstrate that Co^{II}-H is the active species for hydrogen evolution (Fig. 4), in accord with recent experimental (61, 62) and theoretical work (41–43). The relatively slow evolution of H₂ in the reaction of **2** with TsOH•H₂O is a consequence of the slow reduction of **4** by **2**, owing to inadequate driving force coupled with large electrostatic and reorganization barriers associated with the Co^{III/II}-H couple (35). An analogous reaction pathway is operative in H₂ evolution reactions driven by Co^I-diglyoxime complexes. In this case, however, the rate constant for Co^{III}-H reduction by Co^I (9 × 10⁶ M⁻¹ s⁻¹) is about eight orders of magnitude greater than that of the corresponding Co-triphos reaction. We cannot eliminate Co^{III}-H bond homolysis, producing Co^{II} and H₂, as a viable reaction path, but our homogeneous kinetics measurements show that the specific rate of this reaction is at least a factor of 20 smaller than that of Co^{III}-H reduction by Co^I.

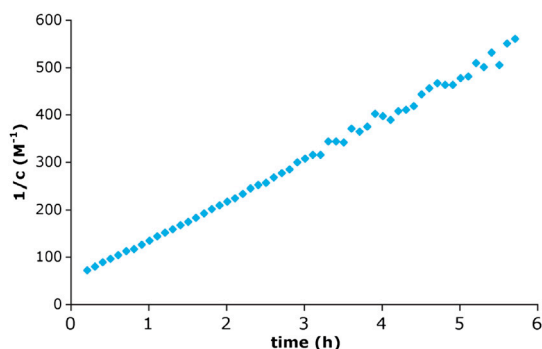


Fig. 3. Kinetics of Co^{III}-H decay measured using ¹H NMR spectroscopy; [Co]₀ = 16.4 mM; [acid]₀ = 0.164 M; 0.7 mL MeCN-d₃.

Conclusions

The failure of Co^{III}-H to evolve H₂ heterolytically in the presence of acid is attributable to unfavorable thermodynamics associated with formation of Co^{III}. The Co^{III/II} reduction potentials in the glyoxime and triphos complexes are more than 0.5 V positive than the Co^{II/I} couples, which are within 100 mV of the HA/H₂ reduction potentials. The reduction of HA by Co^I with concomitant formation of Co^{III} and H₂ is energetically highly unfavorable and can be driven only by subsequent reduction of Co^{III} to Co^{II}.

A sufficiently negative reduction potential is not the sole criterion for H₂ evolution from Co complexes. Prior investigations of a PP₃ triphos complex revealed that exposure of [(PP₃)Co^I(H)] to strong acid leads to a Co^{III} dihydride complex rather than H₂ (48–50). This behavior can be explained by the extreme proton basicity of [(PP₃)Co⁻¹]: double protonation to form [(PP₃)Co^{III}(H)₂] has a greater thermodynamic driving force than reduction of HA to H₂. This behavior illustrates a key requirement of hydrogen evolution chemistry: The reduced metal complex must be sufficiently basic to deprotonate the acid, but if it is too basic the metal hydride intermediate will be too stable, inhibiting hydrogen formation.

A single-metal catalyst for the reduction of protons to hydrogen must utilize two redox couples. For hydrogen formation to be spontaneous, the average of the reduction potentials for the two

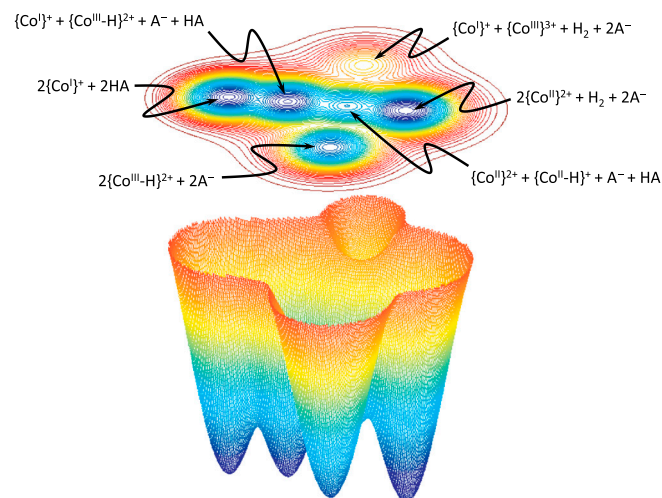


Fig. 4. Schematic energy landscape for H₂ evolution from Co^I (**2**) and TsOH•H₂O (HA). The vertical dimension in the plot corresponds to free energy; the lateral dimensions represent different routes through configuration space. The lowest energy pathway involves nearly isoenergetic protonation of {Co^I}⁺, producing the common intermediate {Co^{III}-H}²⁺ (**4**). Endergonic reduction by {Co^I}⁺ generates a highly reactive hydride, {Co^{II}-H}⁺, that produces H₂ upon reaction with a second equivalent of HA. Overprotonation of {Co^I}⁺ traps the metal complex as {Co^{III}-H}²⁺, from which only a high-energy bimolecular pathway is available for the production of {Co^{II}}²⁺ (**3**) and H₂. Protonation of {Co^{III}-H}²⁺ is an unfavorable pathway, owing to formation of a high-energy {Co^{III}}³⁺ intermediate.

couples must be more negative than the HA/H₂ couple (63). To minimize the overpotential for catalysis, the difference between the two metal-based potentials should be as small as possible. The latter can be accomplished through the sequence reduction-protonation-reduction, wherein the protonation step helps moderate the potential for delivery of the second electron. In the case of Co triphos and glyoxime complexes, our research indicates that the Co^{II/I} and Co^{III}-H/Co^{II}-H couples are extremely well suited for catalysis of hydrogen evolution from acid (41).

Materials and Methods

General. All manipulations of air- and moisture-sensitive materials were conducted under a nitrogen atmosphere in a Vacuum Atmospheres glovebox or on a dual-manifold Schlenk line. The glassware, including NMR tubes, were oven dried prior to use. Diethylether, tetrahydrofuran, dichloromethane, and acetonitrile were degassed and passed through activated alumina columns and stored over 4 Å Linde-type molecular sieves. The deuterated solvents were purchased from Cambridge Isotope Laboratories, Inc., and were dried over 4 Å Linde-type molecular sieves prior to use. The ¹H spectra were acquired at room temperature unless otherwise noted through the use of Varian spectrometers and referenced to the residual ¹H resonances of the deuterated solvent (¹H: CD₂Cl₂, δ 5.32; CD₃CN, δ 1.94) and are reported as parts per million relative to tetramethylsilane. The ³¹P{¹H} NMR spectra were referenced to external phosphoric acid at δ 0 ppm. The ¹⁹F{¹H} NMR spectra were referenced to external fluorobenzene at δ -113.15 ppm. Triphos and CoI₂ were purchased from Sigma-Aldrich and used without further purification. The elemental analyses were performed by Midwest Microlabs.

Cyclic Voltammetry. Electrochemical measurements were recorded in a nitrogen glovebox at 25 °C with a Pine Instruments WaveNow potentiostat. Electrochemical analyses were carried out in a three-electrode cell, consisting of a glassy carbon working electrode (surface area = 0.07 cm²), a platinum wire counter electrode, and a silver wire reference electrode. For all electro-

chemical measurements, the electrolyte solution was 0.1 M [*n*Bu₄N][PF₆]. At the end of each experiment, ferrocene was added to the electrolyte solution and the ferrocenium/ferrocene couple was used to calibrate the reference electrode. In the case of acid titration cyclic voltammetry experiments, a frit separated silver wire reference electrode was used, and the ferrocene was added to the electrolyte solution at the beginning of the experiment.

NMR Measurements. A 0.7 mL MeCN-*d*₃ stock solution of **2** (16.4 mM) and dihydroanthracene (4.1 mM) was added to a 1 dram vial, which was charged with the corresponding amount of *p*-toluenesulfonic acid monohydrate. The reaction mixture was then transferred to a J. Young tube. Reaction progress was monitored by ¹H NMR spectroscopy at the corresponding temperature, where integral areas of Co^{III}-H (δ -7.64 ppm, dt, 1H, *J*_{Pcis-H} = 65 Hz; *J*_{Ptrans-H} = 130 Hz) relative to the aliphatic protons of dihydroanthracene internal standard (δ 3.9 ppm, s, 4H) were obtained at intervals of 2 min (SI Appendix, Fig. S18).

A 0.7 mL MeCN stock solution of **2** (16.4 mM) was added to a 1 dram vial, which was charged with the corresponding amount of *p*-toluenesulfonic acid monohydrate. The reaction mixture was then transferred to a J. Young tube, charged with a sealed capillary tube with Ph₄PBr (8.2 mM). Reaction progress was monitored by ³¹P{¹H} NMR spectroscopy at 25 °C, where integral areas of the phosphorous peaks in [(triphos)Co^{III}-H]²⁺ (δ 37.3 ppm, 2P, Co-P_{cis}) relative to the Ph₄PBr internal standard (δ 24.4 ppm, s, 1P) were obtained at intervals of 4 min.

ACKNOWLEDGMENTS. We thank Lawrence M. Henling and the late Dr. Michael W. Day for crystallographic assistance, and Dr. Jay A. Labinger for insightful comments. Our work is supported by the National Science Foundation Center for Chemical Innovation in Solar Fuels (CHE-0802907); Center for Chemical Innovation postdoctoral fellowship to S.C.M. We thank Chevron-Phillips for additional support. The Bruker KAPPA APEX II X-ray diffractometer was purchased via a National Science Foundation Chemistry Research Instrumentation and Facilities: Departmental Multi-User Instrumentation (CRIF:MU) award to the California Institute of Technology, CHE-0639094.

- Lewis NS, Nocera DG (2006) Powering the planet: Chemical challenges in solar energy utilization. *Proc Natl Acad Sci USA* 103:15729–15735.
- Turner JA (2004) Sustainable hydrogen production. *Science* 305:972–974.
- Gray HB (2009) Powering the planet with solar fuel. *Nat Chem* 1:7.
- Eisenberg R, Nocera DG (2005) Preface: Overview of the forum on solar and renewable energy. *Inorg Chem* 44:6799–6801.
- Frey M (2002) Hydrogenases: Hydrogen-activating enzymes. *ChemBiochem* 3:153–160.
- Fontecilla-Camps JC, Volbeda A, Cavazza C, Nicolet Y (2007) Structure/function relationships of [NiFe]- and [FeFe]-hydrogenases. *Chem Rev* 107:4273–4303.
- Darensbourg MY, Lyon EJ, Smee JJ (2000) The bio-organometallic chemistry of active site iron in hydrogenases. *Coord Chem Rev* 206:533–561.
- Marr AC, Spencer DJE, Schroder M (2001) Structural mimics for the active site of [NiFe] hydrogenase. *Coord Chem Rev* 219:1055–1074.
- Darensbourg MY, Lyon EJ, Zhao X, Georgakaki IP (2003) The organometallic active site of [Fe]hydrogenase: Models and entatic states. *Proc Natl Acad Sci USA* 100:3683–3688.
- Evans DJ, Pickett CJ (2003) Chemistry and the hydrogenases. *Chem Soc Rev* 32:268–275.
- Artero V, Fontecave M (2005) Some general principles for designing electrocatalysts with hydrogenase activity. *Coord Chem Rev* 249:1518–1535.
- Helm ML, Stewart MP, Bullock RM, DuBois MR, DuBois DL (2011) A synthetic nickel electrocatalyst with a turnover frequency above 100,000 s⁻¹ for H₂ production. *Science* 333:863–866.
- Wilson AD, et al. (2007) Nature of hydrogen interactions with Ni(II) complexes containing cyclic phosphine ligands with pendant nitrogen bases. *Proc Natl Acad Sci USA* 104:6951–6956.
- DuBois MR, DuBois DL (2009) The roles of the first and second coordination spheres in the design of molecular catalysts for H₂ production and oxidation. *Chem Soc Rev* 38:62–72.
- Dubois MR, Dubois DL (2009) Development of molecular electrocatalysts for CO₂ reduction and H₂ production/oxidation. *Acc Chem Res* 42:1974–1982.
- Connolly P, Espenson JH (1986) Cobalt-catalyzed evolution of molecular-hydrogen. *Inorg Chem* 25:2684–2688.
- Hu XL, Cossairt BM, Brunschwig BS, Lewis NS, Peters JC (2005) Electrocatalytic hydrogen evolution by cobalt difluoroboryl-diglyoximate complexes. *Chem Commun* 37:4723–4725.
- Hu X, Brunschwig BS, Peters JC (2007) Electrocatalytic hydrogen evolution at low overpotentials by cobalt macrocyclic glyoxime and tetramine complexes. *J Am Chem Soc* 129:8988–8998.
- Dempsey JL, Brunschwig BS, Winkler JR, Gray HB (2009) Hydrogen evolution catalyzed by cobaloximes. *Acc Chem Res* 42:1995–2004.
- Artero V, Chavarot-Kerlidou M, Fontecave M (2011) Splitting water with cobalt. *Angew Chem Int Ed* 50:7238–7266.
- Du P, Eisenberg R (2012) Catalysts made of earth-abundant elements (Co, Ni, Fe) for water splitting: Recent progress and future challenges. *Energy Environ Sci* 5:6012–6021.
- Wang M, Chen L, Sun L (2012) Recent progresses in electrochemical hydrogen production with earth-abundant metal complexes as catalysts. *Energy Environ Sci* 5:6763–6778.
- Jacques P-A, Artero V, Pecaut J, Fontecave M (2009) Cobalt and nickel diimine-dioxime complexes as molecular electrocatalysts for hydrogen evolution with low overvoltages. *Proc Natl Acad Sci USA* 106:20627–20632.
- Stubbert BD, Peters JC, Gray HB (2011) Rapid water reduction to H₂ catalyzed by a cobalt bis(iminopyridine) complex. *J Am Chem Soc* 133:18070–18073.
- Jacobsen GM, et al. (2008) Hydrogen production using cobalt-based molecular catalysts containing a proton relay in the second coordination sphere. *Energy Environ Sci* 1:167–174.
- Sun Y, et al. (2011) Molecular cobalt pentapyridine catalysts for generating hydrogen from water. *J Am Chem Soc* 133:9212–9215.
- Liu T, Darensbourg MY (2007) A mixed-valent, Fe(II)Fe(I), diiron complex reproduces the unique rotated state of the [FeFe]hydrogenase active site. *J Am Chem Soc* 129:7008–7009.
- Loqaugen F, Rauchfuss TB (2009) Small molecule mimics of hydrogenases: Hydrides and redox. *Chem Soc Rev* 38:100–108.
- Kaur-Ghumaan S, Schwartz L, Lomoth R, Stein M, Ott S (2010) Catalytic hydrogen evolution from mononuclear iron(II) carbonyl complexes as minimal functional models of the [FeFe] hydrogenase active site. *Angew Chem Int Ed* 49:8033–8036.
- Appel AM, DuBois DL, DuBois MR (2005) Molybdenum-sulfur dimers as electrocatalysts for the production of hydrogen at low overpotentials. *J Am Chem Soc* 127:12717–12726.
- Karunadasa HI, Chang CJ, Long JR (2010) A molecular molybdenum-oxo catalyst for generating hydrogen from water. *Nature* 464:1329–1333.
- Karunadasa HI, et al. (2012) A Molecular MoS₂ edge site mimic for catalytic hydrogen generation. *Science* 335:698–702.
- Chao TH, Espenson JH (1978) Mechanism of hydrogen evolution from hydrido-cobaloxime. *J Am Chem Soc* 100:129–133.
- Baffert C, Artero V, Fontecave M (2007) Cobaloximes as functional models for hydrogenases. 2. Proton electroreduction catalyzed by difluoroborylbis(dimethylglyoximate)cobalt(II) complexes in organic media. *Inorg Chem* 46:1817–1824.
- Dempsey JL, Winkler JR, Gray HB (2010) Kinetics of electron transfer reactions of H₂-evolving cobalt diglyoxime catalysts. *J Am Chem Soc* 132:1060–1065.
- Dempsey JL, Winkler JR, Gray HB (2010) Mechanism of H₂ evolution from a photogenerated hydridocobaloxime. *J Am Chem Soc* 132:16774–16776.
- Lazarides T, et al. (2009) Making hydrogen from water using a homogeneous system without noble metals. *J Am Chem Soc* 131:9192–9194.
- Szajna-Fuller E, Bakac A (2010) Catalytic generation of hydrogen with titanium citrate and a macrocyclic cobalt complex. *Eur J Inorg Chem* 2010:2488–2494.
- Bhattacharjee A (2012) Combined experimental-theoretical characterization of the hydrido-cobaloxime [HCo(dmgH)₂(*n*Bu₃)]. *Inorg Chem* 51:7087–7093.
- Schrauzer GN, Holland RJ (1971) Hydridocobaloximes. *J Am Chem Soc* 93:1505–1506.

